Nanoscale

PAPER

View Article Online
View Journal | View Issue

Cite this: *Nanoscale*, 2018, **10**, 20804

Self-assembly of supramolecular nanotubes/microtubes from 3,5-dimethyl-4-iodopyrazole for plasmonic nanoparticle organization†

Shasha Li,[a,b] Rui Liu, [a] Deribachew Bekana, [a,b] Yujian Lai[a,b] and Jingfu Liu *[a,b]

Received 10th September 2018,
Accepted 14th October 2018

DOI: 10.1039/c8nr07372d

rsc.li/nanoscale

Hierarchical super-architectures from small molecule self-assembly have interesting properties and play an indispensable role in many fields. In most cases, a self-assembly process refers to multiple intermolecular interactions among intricately designed building blocks. Here, a supramolecular assembly with a tubular morphology with dimensions ranging from nanometers to micrometers was prepared through self-assembly of 3,5-dimethyl-4-iodopyrazole (DMIP), a molecule with an unprecedented simple structure. As predicted by density functional theory (DFT) calculations, the hydrogen bond and halogen bond interaction energy between DMIP molecules can be up to 32.81 kJ mol^{-1}, which effectively drives DMIP molecules to assemble into fibrils, sheets, and finally, tubular architectures. Intriguingly, the formed tubular structure can be easily removed by heating at 100 °C, enabling the material to function as a disposable template to guide linear organization of nanostructures. As a proof of concept, ordered Au or Ag nanochains with diameters ranging from 18 to 120 nm were facilely prepared in high yield.

Introduction

Hierarchical molecular self-assembly is ubiquitous in nature and plays a crucial role in building well-defined architectures, including vesicles, fibrils, ribbons and tubules.[1–3] In addition to allowing orderly execution of various biological functions, these structures also exhibit great potential for broad technological applications, *e.g.*, as soft scaffolds to precisely mediate metallic nanoparticle (NP) organization.[4–7] The material basis for self-assembly is intramolecular noncovalent interactions (such as hydrogen bonding, halogen bonding, hydrophobic interaction, π···π stacking *etc.*)[8–12] among molecular building blocks, which mainly contain biomolecules (DNA,[13–15] peptides[16–18] and lipids[19,20]), block copolymers,[21–23] bolaform surfactants,[24,25] macrocylic molecules[26] and others.[27–30] Basically, most of these are large molecules with sophisticated structures. This inspired us to develop extremely simple molecular building blocks to form well-defined architectures with desired functionality, and such small molecular monomers possess numerous exceptional merits, such as low cost, easy tailorability and processability.[31–36] In addition, as soft templates, the small molecules can be easily removed by external stimuli, such as heating. Moreover, the ability to develop structurally simple small organic compounds to form complex systems with functionalities beyond those of the constituent components opens the door to new assemblies and applications that can evolve from such architectures.

We speculate that 3,5-dimethyl-4-iodopyrazole (DMIP), a remarkably small molecule, has great potential as a simple molecular building block for hierarchical molecular self-assembly based on the following considerations: (i) DMIP contains an iodine atom and N/N–H groups, which provide intermolecular hydrogen and halogen bonding interactions to drive supramolecular self-assembly; (ii) the appropriate spatial arrangement of these functional groups enables end-to-end interactions and elongates the building blocks into the desired structures; and (iii) density functional theory (DFT) calculations revealed that the two types of hydrogen bonds and one halogen bond in the three-molecule model greatly decrease the system energy, supporting the possibility of hierarchical self-assembly of this simple, one-component building block.

In this study, we report the supramolecular self-assembly of DMIP, which is believed to be the simplest molecular building block reported so far, into novel, hollow tubular structures spanning a wide range of spatial scale from nano- to micrometers. In addition, we also highlight the capability of DMIP tubular assemblies to specifically mediate the arrangement of high ordered plasmonic NPs *via* Au/Ag–I bonds. The remarkable small size and simple structure of this building

[a]*State Key Laboratory of Environmental Chemistry and Ecotoxicology, Research Center for Eco-Environmental Sciences, Chinese Academy of Sciences, P.O. Box 2871, Beijing 100085, China. E-mail: jfliu@rcees.ac.cn*
[b]*University of Chinese Academy of Sciences, Beijing 100049, China*
†Electronic supplementary information (ESI) available. See DOI: 10.1039/c8nr07372d

block for complex architecture assembly together with its NP organization ability make this system attractive for research.

Results and discussion

As displayed in Fig. 1a, an evident Tyndall effect was observed in a DMIP ethanol colloid, which is a direct result of DMIP self-assembling into aggregates. The increased light scattering upon the addition of a non-solvent (water) indicated further growth of the DMIP assemblies. With a stepwise increase of water to 70% (v/v), DMIP molecules interconnected into a thermo-reversible opaque gel with a gel–sol transition temperature of 50 °C. The critical gelator concentration detected by the vial inversion test was found to be 60 mM. In addition, rheological measurements (Fig. 1c) manifested a viscoelastic response of the supramolecular gel. The data showed that the values of the storage modulus (G') were greater than those of the loss modulus (G'') over the entire range of frequencies measured, and the moduli were relatively independent of frequency. Besides, it was observed that an increase in DMIP content led to an increase in the storage modulus (G'), which resulted from a growing number of non-covalent cross-linking within the supramolecular gel. Thus, stiffer gels could be achieved by increasing the supramolecular concentrations.

The confocal laser scanning microscopy (CLSM) results of an air-dried gel sample showed fiber-like structures with lengths of several micrometers (Fig. 2a). The inset of Fig. 2a shows a clear contrast image of the assemblies, resulting from the light scattering and reflection by the interior walls and demonstrating the hollow structure of the supramolecular assemblies.[37] The tubular structures were further observed by environmental scanning electron microscopy (ESEM) and atomic force microscopy (AFM). The ESEM analysis allowed us to gain insight into an aligned array of tubular networks with nano- to micrometer widths (Fig. 2c). The cross section of DMIP assemblies, acquired by cutting the assemblies into a few fragments under liquid nitrogen, was visualized. The open-end features demonstrated that the DMIP assemblies were hollow tubules with inhomogeneous inner diameters and wall thicknesses (Fig. 2d and Fig. S1†). The AFM topographic images showed severe tube breakage, which was induced by the solvent evaporation. The cross-section analysis revealed a surface indentation and further confirmed the formation of tubular structures with the height of several nano- to micrometers (Fig. S2†).

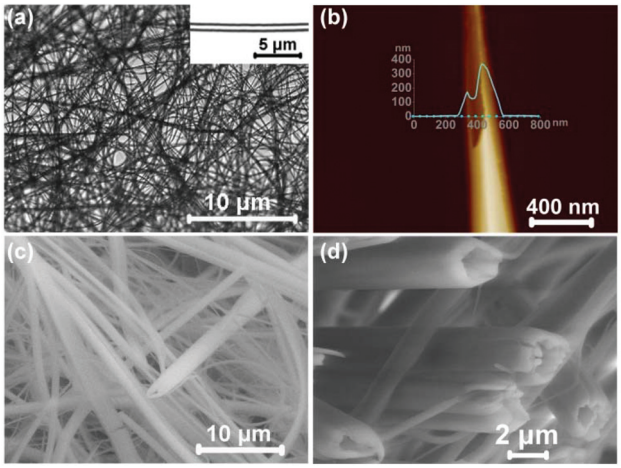

Fig. 2 Optical (a), AFM (b) and ESEM (c and d) images of the DMIP assemblies. The insets in (a) and (b) show one enlarged tubule from (a) and the height profile of the tubule from (b), respectively.

To investigate the intermolecular interaction mechanisms that trigger this unprecedented self-assembly phenomenon, the functional groups in the DMIP molecule were individually exchanged to explore their respective role in this process. As shown in Fig. 3, regardless of removing the iodine atom (3,5-dimethylpyrazole, DMP)/methyl groups (4-iodopyrazole, IP),

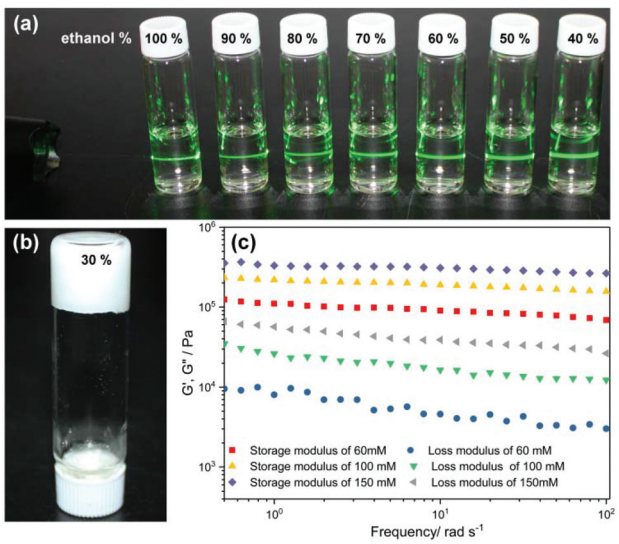

Fig. 1 (a) Tyndall effects of DMIP solutions (100 mM) with different proportions of ethanol and water. (b) Photograph of DMIP gel with 30% ethanol. (c) Frequency sweeps of the supramolecular gel with different concentrations, measured at 0.1% strain.

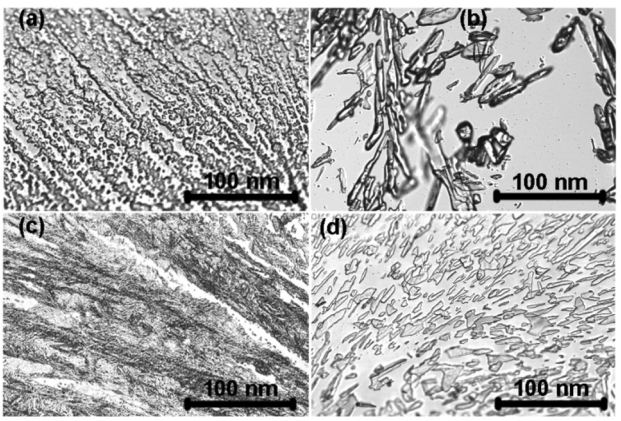

Fig. 3 Optical images of DMP (a), DMBrP (b), TMIP (c) and IP (d).

substituting the iodine atom with a bromine atom (4-bromo-3,5-dimethylpyrazole, DMBrP) or replacing the hydrogen atom bonded to the nitrogen with a methyl group (4-iodo-1,3,5-trimethyl-1*H*-pyrazole, TMIP), only poorly structured architectures, *i.e.*, shorter lengths or less uniform sizes, were formed, suggesting the significant role of the N–H/I/CH_3 groups in the tube formation.

To better understand the intermolecular binding patterns involved in this self-assembly process, the tubules were thoroughly characterized with spectroscopic techniques, including Raman spectroscopy, ^{13}C nuclear magnetic resonance (NMR) and X-ray photoelectron spectroscopy (XPS). The Raman spectra in Fig. 4a1–a3 depict the vibrational differences of the self-assembled DMIP and the non-self-assembled states of DMP and DMBrP. The frequency assignments refer to that of DMP reported in the previous literature.[38] The peak at approximately 3200 cm^{-1} (DMP and DMBrP), which is characteristic of the non-hydrogen-bonded N–H stretching mode, redshifted to 3168 cm^{-1} in the DMIP assemblies, implying the formation of intermolecular hydrogen bonds. Moreover, the frequencies of the C–H stretching modes in the region of 2800–3115 cm^{-1} shifted to lower frequencies, possibly due to their participation in van der Waals interactions. The band at 257 cm^{-1} was ascribed to the C–I stretching modes in DMIP, which is consistent with the results of other iodine-substituted compounds; *i.e.*, the stretching vibrations were assigned to the band at 265 cm^{-1} in 2-iodobenzyl alcohols[39] and 268 cm^{-1} in 1,2-diiodotetrafluoroethane.[40] The redshift of DMIP was attributed to the n → σ* electron donation from the N to I atom, implying C–I involvement in halogen bonding.

The intermolecular halogen bond was further verified by ^{13}C NMR and XPS studies. Since DMIP gel in methanol/water and ethanol/water produced similar morphologies, and halogen bonds also contributed to the formation of supramolecular assemblies for DMIP in methanol/water (Fig. S3†), CD_3OD/D_2O was used for NMR study. Fig. 4b shows that no chemical shift was observed for the carbon attached to iodine as the temperature increased from 25 °C to 40 °C because DMIP is in the gel state within this temperature range, but the signal of that carbon sharply downshifted when the temperature surpassed the gel–sol transition temperature, *i.e.*, 50 °C. At this temperature, the intermolecular halogen bonding was destroyed, resulting in the transition from a gel to a sol. The observed chemical shifts for the iodine-bearing carbon were consistent with similar interactions in the literature.[41–43] Moreover, a control experiment with DMBrP/DMP (Fig. S4†) further proved the contribution of the halogen bonds to the self-assembled 3D network. An XPS analysis was also performed to directly identify halogen bonding in the supramolecular complexes.[44–47] The spectra in the I 3d region for the self-assembled DMIP are depicted in Fig. 4c. Interestingly, two-well resolved doublet peaks were observed, clearly illustrating the presence of two iodine species with chemically distinct environments. The first predominant peak located at 621.0 eV/632.5 eV is characteristic of an unbound iodine group. The second one at a lower binding energy of 618.9 eV/630.4 eV

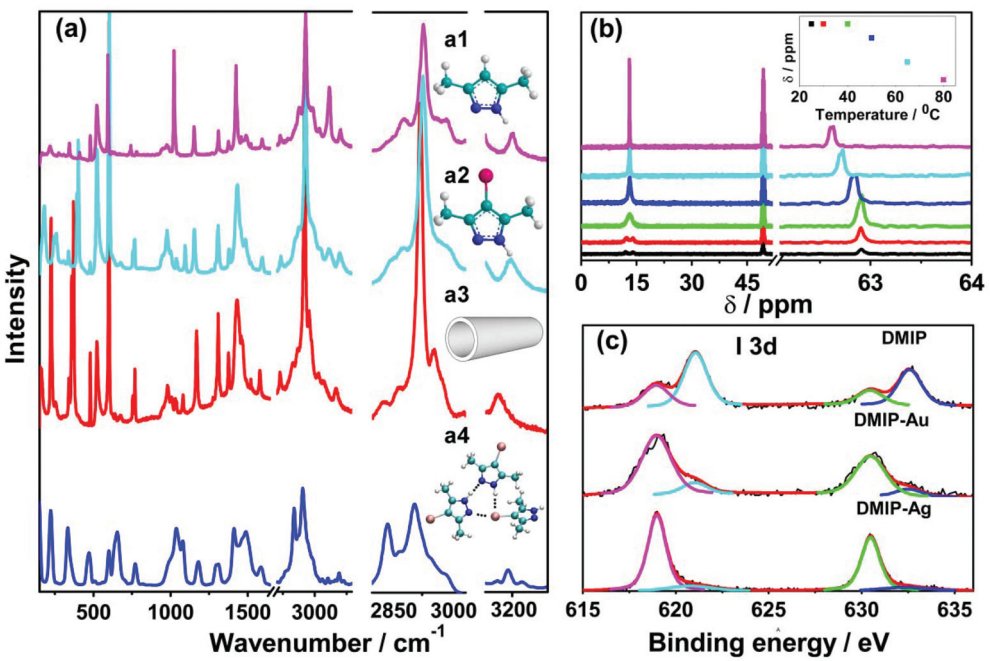

Fig. 4 (a) Experimental Raman spectra of DMP (a1), DMBrP (a2) and self-assembled DMIP tubules (a3). Calculated three-molecule DMIP (minimal self-assembly unit) powder spectrum (a4). (b) Change in the ^{13}C NMR chemical shift of a DMIP hydrogel in CD_3OD/D_2O as the temperature increases from 20 to 80 °C. The inset shows the temperature-dependent changes of the iodine-bound carbon atom of DMIP. (c) XPS spectra of I 3d for DMIP, DMIP-Au and DMIP-Ag.

belongs to chemisorbed iodine, indicating the involvement of iodine in halogen bonding. The Raman spectral modifications, temperature-dependent ^{13}C NMR analysis and XPS results verified that intermolecular hydrogen bonds and halogen bonds act as driving forces to promote the formation of supramolecular tubular architectures.

To gain more insight, we terminated the propagation by quenching a hot DMIP solution with liquid nitrogen. As a result, flexible sheets (Fig. 5b) and partially coiled fragments of tubules (Fig. 5c) were captured. In addition, the broken tubule in Fig. 5a showed fiber-associated tubular structures. These observations suggested the formation of intermediates (fibers, sheets and coiled sheets) before complete tubular structure fabrication. Thus, a preliminary microscopic mechanism has been suggested for the formation process of tubular assemblies, in which the aggregation of DMIP molecules resulted in the formation of supramolecular fibers in the early stages of self-assembly. Then, fibers were packed together side by side to yield sheet-like structures that finally scroll up to form tubular assemblies. The association of fibers into sheets[48,49] and the final step of rolling up[50,51] are similar to what was previously identified in the formation of tubular structures.

Afterwards, DFT calculations were performed to propose the possible molecular model for the assembly process. It was known that the iodine atom possesses two chemical environments; *i.e.*, the top site of the iodine atom possesses a positive charge, and the peripheral site is negatively charged, providing perfect active sites for a halogen bond and additional hydrogen bond.[52] Therefore, we considered three DMIP molecules as the basic self-assembly unit, which was composed of a halogen bond between I–C and N and two types of hydrogen bonds (one between H–N and N and another between H–N and I–C). The DFT results showed that the intermolecular hydrogen and halogen bonds among the three DMIP molecules have an energy of 32.81 kJ mol^{-1}, which is more stable than that of the other four configurations (11.10 kJ mol^{-1}, 11.48 kJ mol^{-1}, 21.90 kJ mol^{-1}, and 32.71 kJ mol^{-1} in Fig. S5†). Further verification was performed by *ab initio* molecular dynamics (AIMD) analysis, which demonstrated that the three-molecule system remained intact during the dynamic process (Movie S1 in the ESI†). The hydrogen bond and halogen bond have always co-existed during the propagation. Moreover, as shown in Fig. 4a3,a4, the calculated vibrational frequencies for the three-molecule system were in good agreement with the actual Raman spectra of DMIP assemblies. Thus, we believe that the halogen bond and hydrogen bond co-assisting structure predominantly contributed to the self-assembly process. As shown in our three-molecule model, there were two I atoms exposed in the structure, which allows growing along the mol2 and mol3 to form fibers. As can be seen from the linear structure, more I atoms were exposed to the surroundings of fibers. Therefore, we speculate that parallel-aligned fibers were associated with each other *via* I···I interaction to create sheets. Although it is not yet fully understood, we consider that the strong directionality of the halogen bond is possibly responsible for the association of fibers two dimensionally, instead of three dimensionally or randomly. Afterwards, due to the high surface areas of the sheets, they have a high tendency to scroll up to yield supramolecular tubules, thus minimizing the surface energy of the system.

The supramolecular tube-like architectures with partial functionally free iodine groups were expected to be a promising scaffold for NP assembly. To verify this, Au NPs (65.3 ± 4.7 nm) stabilized with polyvinyl pyrrolidone (PVP) were used. The assembly could be simply obtained by mixing DMIP and Au NPs in ethanol. Surprisingly, a highly ordered and well-separated array of tube-shaped DMIP/Au NPs with lengths of several micrometers was produced (Fig. 6a and S6†). Some organic tubules were visible, as indicated by the blue arrow in Fig. S7,† while most of them were not visible because DMIP

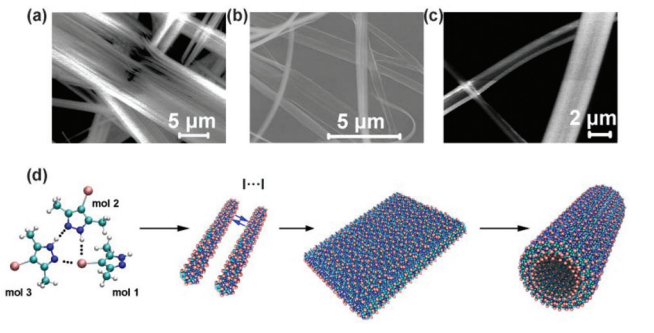

Fig. 5 ESEM images of broken DMIP tubes (a) and the sheets and a partially coiled sheet captured *via* liquid nitrogen (b and c). (d) Proposed model of the DMIP self-assembly formation process of hollow tubular structures.

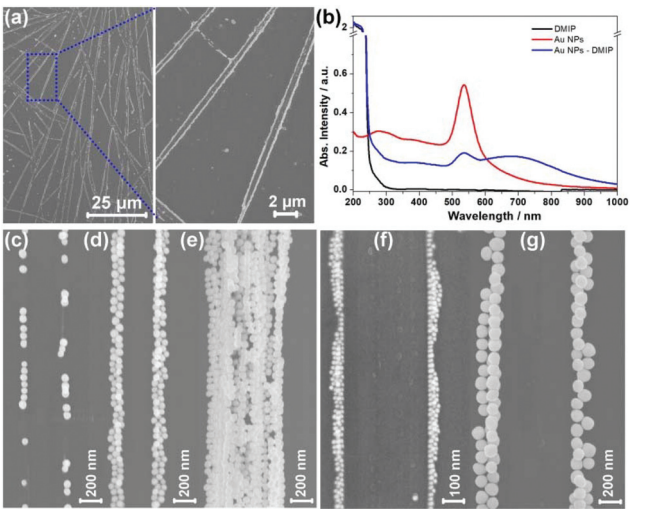

Fig. 6 (a) ESEM images of Au NPs assembled on DMIP tubules. (b) UV-vis absorption spectra of the DMIP assemblies, Au NPs and a mixture of Au NPs and DMIP. (c–g) ESEM images of tubule-shaped DMIP/Au NP nanocomposites with different loading densities and sizes of Au NPs. The concentrations of Au NPs (65.3 nm) are (c) 4.0 mM, (d) 9.5 mM, and (e) 19.0 mM, and the sizes are 18.2 nm (f) and 120.0 nm (g).

was evaporated under high vacuum in the sample chamber of a field emission scanning electron microscope (FESEM). The UV–vis absorption spectrum of the free Au NPs showed a resonance band at 526 nm. Upon mixing with DMIP, the band decreased, and a new peak appeared at 700 nm (Fig. 6b). This band was attributed to longitudinal plasmon coupling, demonstrating the formation of one-dimensional (1D) nanochains.

The surface coverage of Au NPs on the DMIP tubules was easily regulated by altering the concentration of Au NPs. Fig. 6c–e show that the Au NPs appeared to be more densely packed along the organic templates as the concentration of the Au NPs increased. We expected that AuNPs would enter inside the organic tubes. However, in contrast to our expectation, at lower concentrations (4.0 mM and 9.5 mM), the Au NPs were preferentially attached to the external edge of the supramolecular tubes, and a further increase in the Au NP concentration to 19.0 mM resulted in NPs binding to the surface of the tubes. As shown in Fig. S8a,† the organized Au chains showed total closure on one side of the array. Therefore, we surmise that during the organization, NPs may selectively accumulate at the open edges of the supramolecular tubes, and thus other NPs were aligned along the external edge apart from entering into the tubules, which is corroborated by Fig. S8b,c.† Additionally, the ability of the DMIP tubes to mediate the linear assembly of Au NPs with different sizes is significant. Fig. 6d, f, and g illustrate the ESEM images of self-assembled Au NP chains ranging from 18.2 nm to 120.0 nm. To our knowledge, this is the first example of a successful 1D arrangement of large NPs with sizes up to 120.0 nm. Previous attempts at template-directed assembly have been limited primarily to NPs with small sizes (less than 25 nm).[53–57] The previous failure to order large NPs was attributed to geometric restriction or mismatched NP and template sizes. More importantly, the DMIP template can be easily removed by heating to approximately 100 °C without collapsing the NP arrays, which was visualized in the ESEM images (Fig. S9†). The elimination of the supramolecular scaffolds was confirmed from the XPS spectra in the I 3d regions. The intensities of the peaks of I $3d_{5/2}$ and I $3d_{3/2}$ significantly decreased, and minimal DMIP remained adsorbed on the surface of the NPs. Notably, in addition to the Au NPs, the linear arrangement of PVP-capped Ag NPs (110 ± 9.7 nm) was also realized under the same conditions (Fig. S10†), suggesting the versatility of this approach.

The above results reveal that Au/Ag NPs have a strong interaction with the DMIP tubules. The strong interaction is supposed to be related to the subtle interaction of the exposed iodine groups on the surface of the supramolecular template and Au/Ag, which was confirmed by STEM-EDS analysis. STEM-EDS data and STEM-EDS elemental mappings (Fig. S11 and S12†) of DMIP tubule-shaped Au/Ag NP arrays reveal the presence of iodine as one of the components along with Ag/Au. In addition, a straightforward strategy to achieve a better understanding of the significant role of iodine groups in the linear assembly of Au/Ag NPs entails performing XPS analysis that helps verify the existence of chemisorbed iodine on the NP surface and identify the binding nature of this iodine-containing compound with these NPs. To our knowledge, previous associations of NPs with a supramolecular template to create a well-defined inorganic nanostructure assembly have mainly focused on H bonding,[58] thiol anchoring[59,60] or van der Waals interactions.[55] No study has concentrated on the iodine group, which acts as a linker to align the NP arrays. In our work, the iodine spectrum depicted in Fig. 4c exhibited a rise in intensities of the peaks at 618.9 eV/630.4 eV assigned to bonded iodine when DMIP was mixed with Au/Ag NPs, supporting the view that the alignment of the NPs was implemented by the chemisorption of non-bonded iodine in a self-assembled DMIP template to Au/Ag. The peak assignments for chemisorption of iodine to Au/Ag NPs were consistent with those reported in the reference spectrum.[61,62] Further evidence was confirmed through the binding energy shift of Au and Ag after the pre-treatment with DMIP. The XPS spectra shown in Fig. S13† revealed that the binding energy of Au increased slightly by 0.2 eV compared with the reference of metallic Au, which was in line with the change of the Au–I (adsorbed state) complex reported in the previous literature.[63] Meanwhile, the binding energy values of Ag 3d shifted from 368.09 eV to 367.84 eV also proved the chemisorption of Ag with iodine in DMIP.[64,65] In addition, the failure of Ag@SiO_2 NPs to align along the DMIP tubules (Fig. S14†) further verified that the Au/Ag–I interactions governed the arrangement of NPs (the shell SiO_2 cannot interact with the iodine group). These data lead us to conclude that the self-assembled DMIP could serve as an

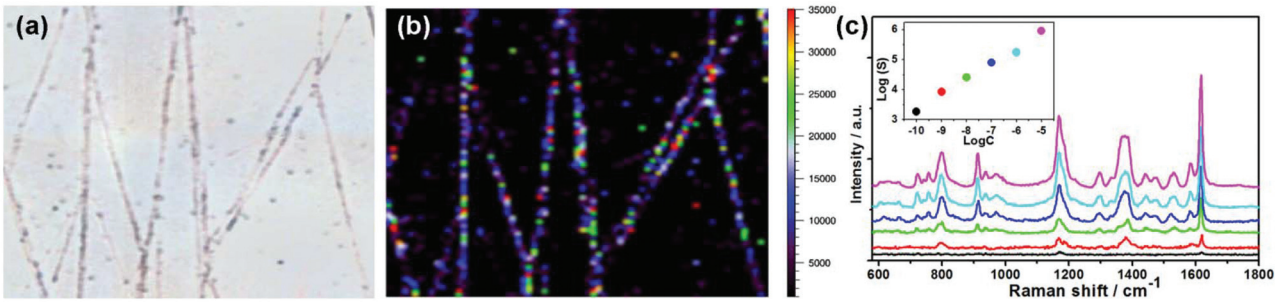

Fig. 7 (a and b) Optical and Raman mapping images at 1619 cm^{-1} excited at 633 nm. (c) SERS spectra of a series of concentrations of CV from 10^{-5} to 10^{-10} ("*S*" means signal intensity).

excellent template to order Au/Ag NPs into well-defined arrays *via* the subtle interaction of iodine with Au/Ag.

The high-level ordered alignment of Au/Ag NPs is astonishing and exhibits great potential for sensing, optoelectronics and catalysis.[66–68] As shown in Fig. 7, the Au assemblies showed an excellent surface-enhanced Raman scattering (SERS) effect. The outline of the Au NP chains was distinctly identifiable against a black background, implying that a high density of "hot spots" was generated along the assembled NP arrays. The SERS activity of the assembled NP arrays was evaluated by preparing a series of concentrations of crystal violet (CV). As can be seen (Fig. 7c), the Raman intensity was augmented with the concentration of CV (1×10^{-5} to 1×10^{-10} M). Discriminable signals for CV were still observed with a concentration as low as 10^{-10} M, indicating the excellent sensitivity of the assembled SERS platform.

Conclusions

In summary, we report the novel ability of DMIP molecules with a very simple structure to self-associate into 1D multiscale structures in the form of nanotubes/microtubes with lengths of several micrometers. Intermolecular hydrogen bonds and halogen bonds drove the molecular self-assembly process. In addition, using these tubular structures as soft templates, we achieved highly ordered plasmonic nanoparticle (*i.e.*, Au and Ag) arrays. The organization achieved with the organic templates was triggered by the presence of unbound iodine groups on the assembled DMIP molecules, thus, providing the possibility for constructing structures with other types of nanoparticles that have affinity for iodine. Moreover, the organic template was easily removed by heating without destroying the NP arrays. This strategy of fabricating such systems not only strengthens our fundamental understanding of self-assembly processes, but also opens a new avenue to construct novel functional materials and devices.

Experimental

Preparation of supramolecular tubes

Typically, the desired amount of DMIP was dissolved in a mixture of ethanol and water (3 : 7, v/v) solution to a concentration of 100 mM by heating until the DMIP powder was completely dissolved. Then, an opaque gel was formed when the hot solution was cooled to room temperature.

Synthesis of Au NPs

Au NPs were synthesized according to a modified literature method.[69] The seed solution for Au NP growth was prepared as follows: 0.5 ml of $HAuCl_4{\cdot}4H_2O$ (0.2% w/v) was added into 50 mL of water, and the resulting solution was heated to boiling. Then, 2 mL of sodium citrate solution (1% w/v) were immediately added under vigorous stirring. After the reaction was finished, some seed solution was added into a three-necked flask. Then, a certain amount of the precursor solution A and reducing solution B was added separately *via* a peristaltic pump at the rate of 0.2 ml min^{-1}. Afterwards, the mixture was heated to boiling for about 30 min. For seeded growth synthesis, in the first step and second step, solution A was prepared by diluting 2 ml of $HAuCl_4{\cdot}4H_2O$ stock solution (0.2% w/v) to 10 mL. Solution B was prepared by diluting 0.5 ml of ascorbic acid stock solution (1% w/v) and 0.25 ml sodium citrate stock solution (1% w/v) to 10 mL. In the third step, solution A was prepared by diluting 8 ml of $HAuCl_4{\cdot}4H_2O$ stock solution (0.2% w/v) to 10 mL and solution B was prepared by diluting 2 ml of ascorbic acid stock solution (1% w/v) and 1 ml sodium citrate stock solution (1% w/v) to 10 mL.

18.2 nm Au NPs: 3 ml seed solutions, 10 ml solution A and 10 ml solution B were used for the synthesis of 18.2 nm Au NPs.

65.3 nm Au NPs: In the first growth step, 3 ml seed solution, 10 ml solution A and 10 ml solution B were used. In the second growth step, 4.5 ml of the last resulting solution, 10 ml solution A and 10 ml solution B were used. In the third growth step, 20 mL of the last solution was used with 10 ml solution A and 10 ml solution B.

120.0 nm Au NPs: In the first growth step, 3 ml seed solution, 10 ml solution A and 10 ml solution B were used. In the second growth step, 5 ml of the last resulting solution, 10 ml solution A and 10 ml solution B were used. In the third growth step, 15 mL of the last solution was used with 11 ml solution A and 11 ml solution B.

To disperse Au NPs in an organic solvent, citrate residues on the surface of the Au core were converted into PVP through site-exchange reactions. After that, Au NPs were washed several times with ethanol by centrifugation and then re-dispersed in ethanol.

Synthesis of Ag NPs

Ag NPs were synthesized according to a modified literature method.[70] The seed solutions were prepared as follows: 50 ml of glycerol/water solution (46% glycerol) were added in a 100 ml flask at 104 °C under vigorous stirring. Then, 10 mg of sodium citrate dissolved in 1 ml water were added in the last solution. After that, 1 ml of $AgNO_3$ aqueous solution (0.5%, w/v) was added. The reaction proceeded for 1 h. For the 110 nm Ag NPs, 0.58 g of PVP and 23 ml glycerol were added to 138 ml water, and then 2.5 ml of seed solutions were added under vigorous stirring. Afterwards, 1.15 ml of diamine silver complex (20 mg $AgNO_3$, 0.22 ml ammonium hydroxide (25%) solution and 1 ml water) were immediately added to the flask with 92 ml aqueous solution (containing 36.8 mg ascorbic acid). The reaction was finished after 1 h. After that, Ag NPs were washed several times with ethanol by centrifugation and then re-dispersed in ethanol.

Templated assembly of Au/Ag NPs on supramolecular structures

A suspension of DMIP (10 μl, 500 mM) and Au/Ag NP (40 μl, 4.0–19.0 mM) ethanol solution were mixed under sonication at

35 °C for 10 min or shaking at room temperature for a night. The resulting mixture was dropcast onto silicon wafers to allow the solvent to evaporate at 4 °C, and visualized with FESEM.

Theoretical calculation

Density functional theory calculation was conducted using the CP2K package[71] to gain insights into the minimal self-assembly unit. Kohn–Sham DFT has been used as the electronic structure method in the framework of the Gaussian and plane waves method.[72] The Goedecker–Teter–Hutter (GTH) pseudopotentials and[73] DZVP-MOLOPT-GTH basis sets[74] were used to describe the molecules. A plane-wave energy cut-off of 500 Ry has been employed.

We define the interaction energy per molecule using the equation below, which can describe the stability of the multiple molecules interaction.

$$E_{\text{int}} = -(E_{\text{nmol}} - n \times E_{\text{mol}})/n$$

The power spectra were calculated using the mass-weighted velocity autocorrelation function.

$$P(\omega) = m \int \langle \dot{r}(\tau)\dot{r}(t+\tau)\rangle_{\tau} e^{-i\omega t} \mathrm{d}t$$

Characterization

Rheological measurements were conducted on a TA rheometer (ARES-G2) with an 8 mm parallel plate. The morphologies of the supramolecular tubular structures and tube-shaped Au/Ag superstructures were characterized using optical microscopy (Zeiss TCS SP5 microscope), atomic force microscopy (AFM, Bruker MultiMode8 and Agilent 5500 microscope), environmental scanning electron microscopy (ESEM, Quanta FEG 250) and field emission scanning electron microscopy (FESEM, Quanta FEG 250). AFM measurements were operated in the tapping mode. Raman spectra were recorded at room temperature on a RenishawInVia Raman microscope equipped with 532 and 633 laser lines as the excitation source. ^{13}C NMR spectra of DMIP gel were obtained on a Bruker AVIII 500WB spectrometer. The chemical state was probed by X-ray photoelectron spectroscopy (XPS) analysis on an ESCALAB 250Xi. UV-vis measurement was conducted with a Shimadzu 3600 UV-Vis-NIR spectrometer.

Conflicts of interest

There are no conflicts to declare.

Acknowledgements

This work was supported by the National Key R&D Program of China (2016YFA0203102), the Strategic Priority Research Program of the Chinese Academy of Sciences (XDB14020101), and the National Natural Science Foundation of China (21337004 and 21620102008). The authors thank Chen-Yang Liu for rheological experiments.

References

1 M. P. Hendricks, K. Sato, L. C. Palmer and S. I. Stupp, *Acc. Chem. Res.*, 2017, **50**, 2440–2448.
2 R. Xiong, H. S. Kim, S. Zhang, S. Kim, V. F. Korolovych, R. Ma, Y. G. Yingling, C. Lu and V. V. Tsukruk, *ACS Nano*, 2017, **11**, 12008–12019.
3 Y. Deng, J. Ling and M.-H. Li, *Nanoscale*, 2018, **10**, 6781–6800.
4 S. H. R. Shin, H. Y. Lee and K. J. Bishop, *Angew. Chem., Int. Ed.*, 2015, **54**, 10816–10820.
5 J. Fang, L. Zhang, J. Li, L. Lu, C. Ma, S. Cheng, Z. Li, Q. Xiong and H. You, *Nat. Commun.*, 2018, **9**, 521.
6 J. Sharma, R. Chhabra, A. Cheng, J. Brownell, Y. Liu and H. Yan, *Science*, 2009, **323**, 112–116.
7 E. Busseron, Y. Ruff, E. Moulin and N. Giuseppone, *Nanoscale*, 2013, **5**, 7098–7140.
8 G. Whitesides, J. Mathias and C. Seto, *Science*, 1991, **254**, 1312–1319.
9 J. Sun, X. Jiang, R. Lund, K. H. Downing, N. P. Balsara and R. N. Zuckermann, *Proc. Natl. Acad. Sci. U. S. A.*, 2016, **113**, 3954–3959.
10 E. Cohen, H. Weissman, I. Pinkas, E. Shimoni, P. Rehak, P. Kral and B. Rybtchinski, *ACS Nano*, 2018, **12**, 317–326.
11 S.-L. Li, T. Xiao, C. Lin and L. Wang, *Chem. Soc. Rev.*, 2012, **41**, 5950–5968.
12 A. M. Smith, R. J. Williams, C. Tang, P. Coppo, R. F. Collins, M. L. Turner, A. Saiani and R. V. Ulijn, *Adv. Mater.*, 2008, **20**, 37–41.
13 J. C. Mitchell, J. R. Harris, J. Malo, J. Bath and A. J. Turberfield, *J. Am. Chem. Soc.*, 2004, **126**, 16342–16343.
14 S. M. Douglas, H. Dietz, T. Liedl, B. Högberg, F. Graf and W. M. Shih, *Nature*, 2009, **459**, 414–418.
15 H. V. P. Thelu, S. K. Albert, M. Golla, N. Krishnan, D. Ram, S. M. Srinivasula and R. Varghese, *Nanoscale*, 2018, **10**, 222–230.
16 X. Gao and H. Matsui, *Adv. Mater.*, 2005, **17**, 2037–2050.
17 J. D. Hartgerink, E. Beniash and S. I. Stupp, *Science*, 2001, **294**, 1684–1688.
18 D. Datta, O. Tiwari and K. N. Ganesh, *Nanoscale*, 2018, **10**, 3212–3224.
19 A. I. Smirnov and O. G. Poluektov, *J. Am. Chem. Soc.*, 2003, **125**, 8434–8435.
20 J. M. Schnur, *Science*, 1993, **262**, 1669–1675.
21 J. Raez, I. Manners and M. A. Winnik, *J. Am. Chem. Soc.*, 2002, **124**, 10381–10395.
22 H. A. Klok and S. Lecommandoux, *Adv. Mater.*, 2001, **13**, 1217–1229.
23 A. Collins, J. Timlin, S. Anthony and G. Montaño, *Nanoscale*, 2016, **8**, 15056–15063.
24 M. Ambrosi, E. Fratini, V. Alfredsson, B. W. Ninham, R. Giorgi, P. Lo Nostro and P. Baglioni, *J. Am. Chem. Soc.*, 2006, **128**, 7209–7214.
25 X. Cheng, F. Liu, X. Zeng, G. Ungar, J. Kain, S. Diele, M. Prehm and C. Tschierske, *J. Am. Chem. Soc.*, 2011, **133**, 7872–7881.

26 W.-Y. Yang, E. Lee and M. Lee, *J. Am. Chem. Soc.*, 2006, **128**, 3484–3485.
27 L. Zang, Y. Che and J. S. Moore, *Acc. Chem. Res.*, 2008, **41**, 1596–1608.
28 V. Palermo and P. Samorì, *Angew. Chem., Int. Ed.*, 2007, **46**, 4428–4432.
29 I. Choi, R. Suntivich, F. A. Plamper, C. V. Synatschke, A. H. Müller and V. V. Tsukruk, *J. Am. Chem. Soc.*, 2011, **133**, 9592–9606.
30 M. Ornatska, S. Peleshanko, B. Rybak, J. Holzmueller and V. V. Tsukruk, *Adv. Mater.*, 2004, **16**, 2206–2212.
31 X. Yan, P. Zhu and J. Li, *Chem. Soc. Rev.*, 2010, **39**, 1877–1890.
32 R. N. Das, Y. P. Kumar, S. Pagoti, A. J. Patil and J. Dash, *Chem. – Eur. J.*, 2012, **18**, 6008–6014.
33 T. Giorgi, S. Lena, P. Mariani, M. A. Cremonini, S. Masiero, S. Pieraccini, J. P. Rabe, P. Samorì, G. P. Spada and G. Gottarelli, *J. Am. Chem. Soc.*, 2003, **125**, 14741–14749.
34 A. M. Kumar, S. Sivakova, J. D. Fox, J. E. Green, R. E. Marchant and S. J. Rowan, *J. Am. Chem. Soc.*, 2008, **130**, 1466–1476.
35 L. E. Buerkle, Z. Li, A. M. Jamieson and S. J. Rowan, *Langmuir*, 2009, **25**, 8833–8840.
36 J. T. Davis and G. P. Spada, *Chem. Soc. Rev.*, 2007, **36**, 296–313.
37 F. Wang, B. Chen, W. Kong, Y. Liu, Y. Lu, M. Li, X. Qiao and X. Fan, *Angew. Chem., Int. Ed.*, 2017, **56**, 10383–10387.
38 N. Sundaraganesan, E. Kavitha, S. Sebastian, J. Cornard and M. Martel, *Spectrochim. Acta, Part A*, 2009, **74**, 788–797.
39 T. Misiaszek, K. Knapik, A. Gągor and M. Trzebiatowska-Gusowska, *J. Mol. Struct.*, 2013, **1054**, 117–122.
40 P. Cardillo, E. Corradi, A. Lunghi, S. V. Meille, M. T. Messina, P. Metrangolo and G. Resnati, *Tetrahedron*, 2000, **56**, 5535–5550.
41 A. Abate, M. Saliba, D. J. Hollman, S. D. Stranks, K. Wojciechowski, R. Avolio, G. Grancini, A. Petrozza and H. J. Snaith, *Nano Lett.*, 2014, **14**, 3247–3254.
42 S. M. Walter, F. Kniep, E. Herdtweck and S. M. Huber, *Angew. Chem., Int. Ed.*, 2011, **50**, 7187–7191.
43 H. G. Loehr, A. Engel, H. P. Josel, F. Voegtle, W. Schuh and H. Puff, *J. Org. Chem.*, 1984, **49**, 1621–1627.
44 N. Houbenov, R. Milani, M. Poutanen, J. Haataja, V. Dichiarante, J. Sainio, J. Ruokolainen, G. Resnati, P. Metrangolo and O. Ikkala, *Nat. Commun.*, 2014, **5**, 4043.
45 L. González, N. l. Gimeno, R. M. Tejedor, V. Polo, M. B. Ros, S. Uriel and J. L. Serrano, *Chem. Mater.*, 2013, **25**, 4503–4510.
46 A. Priimagi, M. Saccone, G. Cavallo, A. Shishido, T. Pilati, P. Metrangolo and G. Resnati, *Adv. Mater.*, 2012, **24**, OP345–OP352.
47 A. Priimagi, G. Cavallo, A. Forni, M. Gorynsztejn–Leben, M. Kaivola, P. Metrangolo, R. Milani, A. Shishido, T. Pilati and G. Resnati, *Adv. Funct. Mater.*, 2012, **22**, 2572–2579.
48 R. Mizuta, J. M. Devos, J. Webster, W. L. Ling, T. Narayanan, A. Round, D. Munnur, E. Mossou, A. A. Farahat, D. W. Boykin, W. D. Wilson, S. Neidle, R. Schweins, P. Rannou, M. Haertlein, V. T. Forsyth and E. P. Mitchell, *Nanoscale*, 2018, **10**, 5550–5558.
49 L. Ziserman, H.-Y. Lee, S. R. Raghavan, A. Mor and D. Danino, *J. Am. Chem. Soc.*, 2011, **133**, 2511–2517.
50 Y. Chen, B. Zhu, F. Zhang, Y. Han and Z. Bo, *Angew. Chem., Int. Ed.*, 2008, **47**, 6015–6018.
51 Z. Shen, T. Wang and M. Liu, *Chem. Commun.*, 2014, **50**, 2096–2099.
52 G. Cavallo, P. Metrangolo, R. Milani, T. Pilati, A. Priimagi, G. Resnati and G. Terraneo, *Chem. Rev.*, 2016, **116**, 2478.
53 J. Majoinen, J. Hassinen, J. S. Haataja, H. T. Rekola, E. Kontturi, M. A. Kostiainen, R. H. Ras, P. Törmä and O. Ikkala, *Adv. Mater.*, 2016, **28**, 5262–5267.
54 O. Deschaume, B. De Roo, M. J. Van Bael, J.-P. Locquet, C. Van Haesendonck and C. Bartic, *Chem. Mater.*, 2014, **26**, 5383–5393.
55 N. M. Sangeetha, C. Blanck, T. T. T. Nguyen, C. Contal and P. J. Mésini, *ACS Nano*, 2012, **6**, 8498–8507.
56 T. Teranishi, A. Sugawara, T. Shimizu and M. Miyake, *J. Am. Chem. Soc.*, 2002, **124**, 4210–4211.
57 P. K. Lo, F. Altvater and H. F. Sleiman, *J. Am. Chem. Soc.*, 2010, **132**, 10212–10214.
58 J. Puigmartí-Luis, Á. Pérez del Pino, E. Laukhina, J. Esquena, V. Laukhin, C. Rovira, J. Vidal-Gancedo, A. G. Kanaras, R. J. Nichols and M. Brust, *Angew. Chem., Int. Ed.*, 2008, **47**, 1861–1865.
59 J. van Herrikhuyzen, S. J. George, M. R. Vos, N. A. Sommerdijk, A. Ajayaghosh, S. C. Meskers and A. P. Schenning, *Angew. Chem., Int. Ed.*, 2007, **46**, 1825–1828.
60 M. Kimura, S. Kobayashi, T. Kuroda, K. Hanabusa and H. Shirai, *Adv. Mater.*, 2004, **16**, 335–338.
61 L. Xiang, T. Hines, J. L. Palma, X. Lu, V. Mujica, M. A. Ratner, G. Zhou and N. Tao, *J. Am. Chem. Soc.*, 2016, **138**, 679–687.
62 G. Eder, E. F. Smith, I. Cebula, W. M. Heckl, P. H. Beton and M. Lackinger, *ACS Nano*, 2013, **7**, 3014–3021.
63 G. Berry, B. Bravo, M. Bothwell, G. Cali, J. Harris, T. Mebrahtu, S. Michelhaugh, J. Rodriguez and M. Soriaga, *Langmuir*, 1989, **5**, 707–713.
64 P. Wang, B. Huang, Q. Zhang, X. Zhang, X. Qin, Y. Dai, J. Zhan, J. Yu, H. Liu and Z. Lou, *Chem. – Eur. J.*, 2010, **16**, 10042–10047.
65 H. Zhang, G. Wang, D. Chen, X. Lv and J. Li, *Chem. Mater.*, 2008, **20**, 6543–6549.
66 J. Zhao and R. Jin, *Nano Today*, 2018, **18**, 86–102.
67 X. Hong, C. Tan, J. Liu, J. Yang, X.-J. Wu, Z. Fan, Z. Luo, J. Chen, X. Zhang and B. Chen, *J. Am. Chem. Soc.*, 2015, **137**, 1444–1447.
68 Z. Liu, Z. Yang, B. Peng, C. Cao, C. Zhang, H. You, Q. Xiong, Z. Li and J. Fang, *Adv. Mater.*, 2014, **26**, 2431–2439.
69 C. Ziegler and A. Eychmüller, *J. Phys. Chem. C*, 2011, **115**, 4502–4506.
70 D. Steinigeweg and S. Schlücker, *Chem. Commun.*, 2012, **48**, 8682–8684.

71 J. Hutter, M. Iannuzzi, F. Schiffmann and J. VandeVondele, *Wiley Interdiscip. Rev.: Comput. Mol. Sci.*, 2014, **4**, 15–25.
72 J. VandeVondele, M. Krack, F. Mohamed, M. Parrinello, T. Chassaing and J. Hutter, *Comput. Phys. Commun.*, 2005, **167**, 103–128.
73 C. Hartwigsen, S. Gœdecker and J. Hutter, *Phys. Rev. B: Condens. Matter Mater. Phys.*, 1998, **58**, 3641.
74 J. VandeVondele and J. Hutter, *J. Chem. Phys.*, 2007, **127**, 114105.